Stability Analysis of a Cracked Blade Coupled with a Rigid Rotor

Bruno R. F. Rende(✉), Izabela B. da Silva, Tobias S. Morais, Aldemir Ap. Cavalini Jr., and Valder Steffen Jr.

LMEst - Structural Mechanics Laboratory, School of Mechanical Engineering, Federal University of Uberlândia, Av. João Naves de Ávila, 2121, Uberlândia, MG 38408-196, Brazil
brunorende@ufu.br

Abstract. Flexible blades coupled to rotating systems are commonly used in industrial machines, such as compressors, exhausters, and turbines. These components are usually exposed to different operating conditions, including high speed, large centrifugal forces, high temperatures, and pressure. Considering the inevitable manufacturing flaws, cracks can emerge and grow particularly in blades of these systems. Thus, investigations on the dynamic behavior of cracked blades become mandatory to prevent failures. In this work, the development, solution, and instability analysis of a system composed of four flexible blades coupled to a flexible shaft are presented. The flexible blades are modeled as Euler-Bernoulli beams with tip masses attached at their ends. Their deformations are obtained by considering second order nonlinear terms to ensure that the centrifugal stiffness is correctly represented, thus characterizing a second order linearized model. The equations of motion are obtained by applying the so-called Newton-Euler-Jourdain method. The crack presence brings an additional flexibility to the blades, which is introduced in the model by using a torsional spring. The resulting blade stiffness is obtained through the beam elastic equation. The Newmark time integration method is associated with the Newton-Raphson iteration procedure to integrate the equations of motion. The system was evaluated for different situations, regarding the depth of the crack in the blades, as well as the operating condition of the rotor-blade system. Finally, the instability map and the vibration responses of the system is determined. The obtained results indicate the instability condition of the rotor-blade system for a certain combination of rotating speed, angular position of the blades, and crack depth.

Keywords: Rotor-blade system · Second order linearized model
Crack · Instability map

1 Introduction

Flexible blades coupled to rotating shafts are widely used in industrial machines, such as compressors, exhausters, and turbines. These components are usually exposed to different operating conditions, including high-speed situations, large centrifugal forces, high temperatures, and high pressures [1]. Thus, associated with the inevitable

K. L. Cavalca and H. I. Weber (Eds.): IFToMM 2018, MMS 62, pp. 178–192, 2019.
https://doi.org/10.1007/978-3-319-99270-9_13

manufacturing flaws and with the possible presence of a foreign object in the system, damage in the system may occur. One of the most dangerous damages is the growth a crack in the blades. This occurs mainly near the attachment between the rotor and the blade. If the crack is not identified it can lead to failure, even to catastrophic consequences. In these cases, the application of predictive maintenance is mandatory.

Nowadays, there are various methods used for crack detection, such as the ultrasonic, X-rays, and acoustic emission [2]. These methods have not proved to be efficient in some situations due to the required detailed periodic inspection, which is very costly [3]. Thus, this problem justified investigations on a class of crack detection methods based on vibration analysis through either frequency or time domain responses.

There are contributions in literature devoted to the modeling of flexible blades. Legrand [4] modeled the blades of a rotor-blade system by using the finite element method, where each finite element was described as Euler-Bernoulli beam. Santos et al. [5] and Saracho [6] used an alternative approach based on the Newton-Euler-Jourdain method to obtain the equations of motion of a rotor-blade system. The authors pointed out that the deformation of the blades cannot be neglected because the coupling between their displacement and deformation causes an effect known as centrifugal stiffening. This effect makes the natural frequencies of the beam increase according to the rotating speed, which is the main characteristic observed in the dynamic behavior of this kind of system.

The dynamic behavior of cantilever beams with transversal cracks was extensively discussed in various papers. Wu and Huang [2] employed an energy approach followed by the Extended Hamilton principle in conjunction with a weighted residual method to obtain the equations of motion of a cracked beam. Dimarogonas [7] and Chondros [8] explained that the crack generates a new local flexibility in the beam. The authors used the linear fracture mechanics theory to represent the crack. Dimarogonas, Rizos, and Aspragathos [9] also observed that the most important effect introduced by cracks on beams is a new local flexibility that changes the dynamical behavior of the system. The authors formulated a model composed of two beams connected by a torsional spring to represent this effect, whose stiffness coefficient represents the crack. The crack strain energy function was used to determine the additional local flexibility on the beam [10]. Mayes and Davies [11] proposed a finite element model to include the new local flexibility in the shaft, in which the diameter of the shaft finite element was reduced at the crack position according to the crack flexibility.

In this context, the present work aims to investigate the influence of cracks on the dynamic behavior of a rotor-blade system based on its vibration responses. In this case, the adopted model for the rotor-blade system is similar to the one described in Saracho [6]. The model is composed of a mass-spring system that represents the rotor and four rotating beams with tip masses attached to them. The blades are modeled as Euler-Bernoulli beams [5] and their deformations were obtained by considering second order non-linear terms to ensure that the centrifugal stiffness is correctly represented [12]. Then, a second order-linearized model was obtained. The Newton-Euler-Jourdain method was applied to determine the equations of motion of the rotor-blade system. The crack is represented by an additional local flexibility of the blade according to the formulation presented in [9].

The equations of motion were solved by using the Newmark time integration method and Newton-Raphson iteration technique by considering different damage scenarios. The first one evaluated the rotor-blade system without crack (pristine condition) and the others considered a crack in one of the blades with different depths. The obtained results indicated the instability condition of the rotor-blade system for a certain combination of rotating speed and crack depth.

2 Mathematical Model

2.1 Rotor-Blade Model

The model used to represent the coupling between the rotor and the four flexible blades is shown in Fig. 1. The system is composed of a rotor with mass m_0 and radius r, which is elastically supported by the stiffness k_0, and four blades with lengths L_i, thickness h_i, and stiffness k_i (i = 1, 2, 3, and 4). Tip masses m_{pi} are attached to the blades, presenting length L_{ti} and width b_{ti}. The distance between the extremity and the centroid of the tip mass is given by r_{ti}. The system has five degrees of freedom $z(t) = \{z_0(t)\ z_1(t)\ z_2(t)\ z_3(t)\ z_4(t)\}^T$, where $z_0(t)$ represents the horizontal displacement of the rotor (point C in Fig. 1) and $z_i(t)$ describes the displacements of the blades.

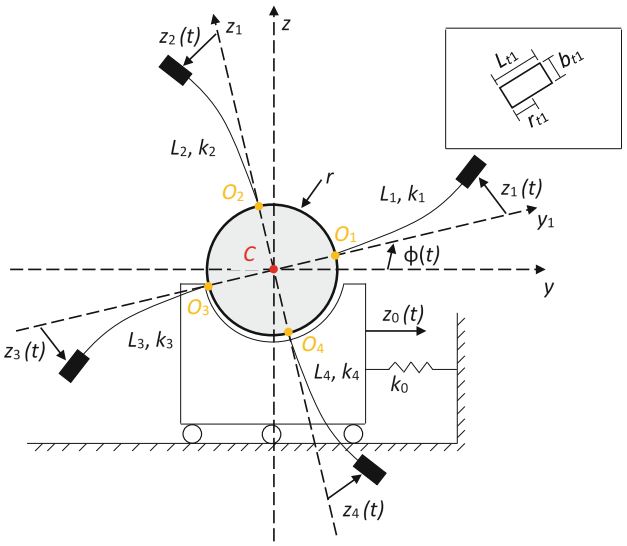

Fig. 1. Model illustrating the rotor-blade system. (Adapted from Santos el al. [5]).

Three reference frames are used to obtain the equations of motion of the rotor-blade system [6], as follows: the inertial frame B_I (x, y, z), the rotating frame B_1 (x_1, y_1, z_1) centered at point C (defining the angular position ϕ through the y_1 axis), and the frame B_{pi} (x_{pi}, y_{pi}, z_{pi}) fixed to each tip mass.

According to Santos et al. [5], the reference frame B_{pi} facilitates the description of the beam deformation field. Therefore, this frame was employed to find the displacements and the external forces of each blade *pi*. The displacements of the blades are interpolated by using a cubic polynomial form to minimize the number of degrees of freedom of the model and to approximate only the first bending mode of the blade [6]. The displacements are shown in Eq. (1).

$$ {}_{B_{pi}}\mathbf{u}_{pi} = \begin{pmatrix} 0 \\ 0 \\ \psi_i(\xi_i) z_i(t) \end{pmatrix} \quad \psi_i(\xi_i) = \frac{3}{2}\left(\frac{\xi_i}{L_i}\right)^2 - \frac{1}{2}\left(\frac{\xi_i}{L_i}\right)^3 \tag{1} $$

Then, the absolute velocity and the acceleration of each blade are given by Eqs. (2) and (3), respectively.

$$ {}_{B_{pi}}\mathbf{v}_{pi} = {}_{B_{pi}}\mathbf{v}_{O_i} + \frac{d}{dt}\left({}_{B_{pi}}\mathbf{u}_i\right) + {}_{B_{pi}}\boldsymbol{\omega}\, x\, \left({}_{B_{pi}}\mathbf{L}_i + {}_{B_{pi}}\mathbf{u}_i\right) \tag{2} $$

$$ \begin{aligned} {}_{B_{pi}}\mathbf{a}_{pi} = {}_{B_{pi}}\mathbf{a}_{O_i} + \frac{d^2}{dt^2}\,{}_{B_{pi}}\mathbf{u}_i + 2{}_{B_{pi}}\boldsymbol{\omega} \times {}_{B_{pi}}\mathbf{u}_i \\ + {}_{B_{pi}}\dot{\boldsymbol{\omega}} \times \left({}_{B_{pi}}\mathbf{L}_i + {}_{B_{pi}}\mathbf{u}_i\right) + {}_{B_{pi}}\boldsymbol{\omega} \times {}_{B_{pi}}\boldsymbol{\omega} \times \left({}_{B_{pi}}\mathbf{L}_i + {}_{B_{pi}}\mathbf{u}_i\right) \end{aligned} \tag{3} $$

where ${}_{Bpi}\mathbf{v}_{pi}$ and ${}_{Bpi}\mathbf{a}_{pi}$ ${}_{Bpi}\boldsymbol{\omega}$ are the velocity and acceleration of the point where the blade is fixed to the rotor (point O_i in Fig. 1), respectively, ${}_{Bpi}\boldsymbol{\omega}$ and ${}_{Bpi}\,\dot{\boldsymbol{\omega}}$ represent the angular speed and acceleration of the rotor, respectively. These vectors are shown in Eq. (4). It is important to note that the only external force applied to the system is the weight.

$$ {}_{B_{pi}}\boldsymbol{\omega} = \begin{Bmatrix} \dot{\varphi} \\ 0 \\ 0 \end{Bmatrix} \quad {}_{B_{pi}}\dot{\boldsymbol{\omega}} = \begin{Bmatrix} \ddot{\varphi} \\ 0 \\ 0 \end{Bmatrix} \quad {}_{B_{pi}}\mathbf{L}_i = \begin{Bmatrix} 0 \\ L_i \\ 0 \end{Bmatrix} \tag{4} $$

In the rotor-blade model, the rotatory inertia was taken into account. Thus, an equivalent mass is estimated as follows:

$$ \begin{aligned} \bar{m}_i &= m_i \psi(L_i)^2 + (I_{ti} + m_i r_{ti})\,\psi'(L_i)^2 + 2 m_i r_{ti} \psi(L_i)\psi'(L_i) \\ I_{ti} &= m_i \left(\frac{L_{ti}^2 + h_{ti}^2}{12}\right) \end{aligned} \tag{5} $$

where $\psi(L_i)$ is the cubical polynomial showed in Eq. (1) and h_{ti} is the height of the tip mass, which will be considered the same height of the blade.

The energy stored in the system was separated in two terms, π_0 that represents the energy of the elastic support and π_{pi}, which is the potential energy of the blades. In this case, $\pi_{pi} = \pi_{li} + \pi_{gi}$, where π_{li} is associated with the blades deformation and π_{gi} is the

energy related to the blade geometrical stiffness. The energy π_{gi} ensures that the second order non-linear terms of the deformation vector are not neglected (see Eqs. (6) to (9)).

$$\pi_0 = \frac{1}{2} k_0 z_0^2 \tag{6}$$

$$\pi_{li} = \frac{1}{2} \int_0^{L_i} EI \left\{ \frac{\partial^2}{\partial \xi_i^2} [\psi_i(\xi_i) z_i] \right\}^2 d\xi_i = \frac{1}{2} k_i z_i^2 \quad k_i = \frac{3EI}{L_i} \tag{7}$$

$$\pi_{gi} = \frac{1}{2} \int_0^{L_i} N_{pi}(\xi_i) \left\{ \frac{\partial^2}{\partial \xi_i^2} [\psi_i(\xi_i) z_i] \right\}^2 d\xi_i = \frac{3}{5L_i} N_{pi}(\xi_i) z_i^2 \tag{8}$$

$$\pi_{pi} = \pi_{li} + \pi_{gi} \tag{9}$$

where N_{pi} is the normal force acting on each blade. The expression of the normal force can be approximated by using Eq. (10) [13].

$$N_{pi}(\xi_i) = m_{pi} \dot{\phi}^2 (L_i + r) \tag{10}$$

The Newton-Euler-Jourdain method is applied to obtain the system equations of motion, as given by Eq. (11). In this case, an eccentricity ε in a given angular position Φ is considered in the model.

$$\mathbf{M}\,\ddot{\mathbf{q}} + \left[\mathbf{C}_1 + \mathbf{C}_p\right] \dot{\mathbf{q}} + \left[\mathbf{K} + \mathbf{K}_\Omega + \mathbf{K}_\alpha + \mathbf{K}_g\right] \mathbf{q} = \mathbf{f}_\Omega + \mathbf{f}_\alpha + \mathbf{f}_p \tag{11}$$

in which $\mathbf{M}$ is the mass matrix, $\mathbf{C}_1$ is the Coriolis matrix, $\mathbf{K}$ represents the structural stiffness matrix, $\mathbf{K}_\Omega$ is the stiffness matrix due to the angular speed, $\mathbf{K}_\alpha$ is the stiffness matrix due to the angular acceleration, $\mathbf{K}_g$ is the geometric stiffness, $\mathbf{f}_\Omega$ is the force vector associated with angular speed, $\mathbf{f}_\alpha$ is the force vector due to angular acceleration, and $\mathbf{f}_p$ is the weight force vector. A proportional damping matrix $\mathbf{C}_p$ was added to the system, as shows Eq. (12).

$$\mathbf{C}_p = \alpha \mathbf{M} + \beta \mathbf{K} \quad \alpha = 5 \quad \beta = 1 \times 10^{-5} \tag{12}$$

2.2 Crack Model

The structural stiffness $\mathbf{K}$ presented in Eq. (11) should be modified due to the local flexibility introduced by the crack. Following Dimarogonas, Rizos, and Aspragathos [9], the blade was separated into two beams (see Fig. 2b) with lengths $L_{B1} = L_1$ and $L_{B2} = L - L_{B1}$. These new beams are also modeled as Euler-Bernoulli beams, linked by a torsional spring with stiffness coefficient k_T.

Equations (13) and (14) present the stiffness coefficient k_T determined according to the crack depth a and position L_{B1} along the blade. In this case, it was considered that the beams had only bending movement.

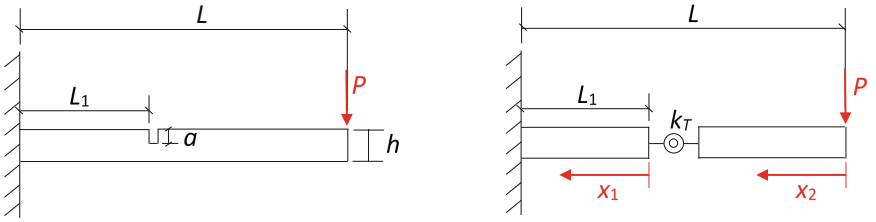

a) Crack depth and beam height. b) Model used to determine the stiffness.

Fig. 2. Schematic model used to represent the crack.

$$k_T = \frac{1}{c} \quad c = \left(\frac{5.346h}{EI}\right) I\left(\frac{a}{h}\right) \tag{13}$$

$$\begin{aligned} I\left(\frac{a}{h}\right) = {} & 1.8624\left(\frac{a}{h}\right)^2 - 3.95\left(\frac{a}{h}\right)^3 + 16.375\left(\frac{a}{h}\right)^4 - 37.226\left(\frac{a}{h}\right)^5 \\ & + 76.81\left(\frac{a}{h}\right)^6 - 126.9\left(\frac{a}{h}\right)^7 + 172\left(\frac{a}{h}\right)^8 - 143.97\left(\frac{a}{h}\right)^9 + 66.56\left(\frac{a}{h}\right)^{10} \end{aligned} \tag{14}$$

where c is the compliance, h is the beam height, E and I are, respectively, the Young's modulus of the material and the moment of inertia of the blade cross section. $I(a/h)$ is the dimensionless local compliance.

As can be seen in Fig. 2, the blade was divided into two beams with lengths L_{B1} and L_{B2}, connected by the angular stiffness k_T to represent the cracked blade. Thus, an equivalent stiffness coefficient was determined by considering the scheme presented in Fig. 2b, as shows Eq. (15).

$$k_{eq} = \frac{1}{\frac{1}{k_{B1}} + \frac{1}{k_{B2}} + \frac{1}{k_T}} \tag{15}$$

where k_{B1} is the stiffness of the beam with length L_{B1} (beam #1) and k_{B2} is the stiffness of the beam with length L_{B2} (beam #2). It is worth mentioning that the coefficients k_{B1} and k_{B2} were obtained by using the Euler-Bernoulli theory through the elastic line equation, as given by:

$$\frac{d^2y_1}{dx_1^2} = \frac{M}{EI} \quad M = Px_1 + PL_{B2} \tag{16}$$

where y is the deflection of the beam, M is the bending moment applied to the beam, and P is a force applied in the end of the beam (see Fig. 2).

Integrating Eq. (16) twice with respect to x_1 ($0 \leq x_1 \leq L_1$), the vertical displacement y_1 and the deflection α_1 of the beam #1 are obtained as follows:

$$y_1 = \frac{Px_1^3}{6EI} + \frac{PL_{B2}x_1^2}{2EI} + C_1x_1 + C_2 \quad \frac{dy_1}{dx_1} = \alpha_1 = \frac{Px_1^2}{2EI} + \frac{PL_{B2}x_1}{EI} + C_1 \tag{17}$$

where C_1 and C_2 are constants that can be evaluated by considering $\alpha_1 = 0$ and $y_1 = 0$ at $x_1 = L_{B1}$. Thus,

$$C_1 = -\frac{P}{EI}\left(\frac{L_{B1}^2}{2} + L_{B1}L_{B2}\right) \quad C_2 = \frac{P}{EI}\left(\frac{L_{B2}L_{B1}^2}{2} + \frac{L_{B1}^3}{3}\right) \tag{18}$$

At $x_1 = 0$, $k_{B1} = P/y_1$. Consequently,

$$k_{B1} = \frac{EI}{\left(\frac{L_{B2}L_{B1}^2}{2} + \frac{L_{B1}^3}{3}\right)} \tag{19}$$

The stiffness k_{B2} of the beam #2 can be found by using a similar procedure through Eq. (16). Then, for the beam #2 (Fig. 2b), with $0 \leq x_2 \leq L_2$:

$$\frac{d^2y_2}{dx_2^2} = \frac{M}{EI} \quad M = Px_2 \tag{20}$$

Integrating Eq. (20) twice with respect to x_2, the displacement y_2 and deflection α_2 can be obtained as follows:

$$\begin{aligned} y_2 &= \frac{Px_2}{2EI} + C_3x_2 + C_4 \\ \frac{dy_2}{dx_2} &= \alpha_2 = \frac{Px_2}{2EI} + C_3 \end{aligned} \tag{21}$$

The constants C_3 and C_4 in Eq. (22) are determined by using the boundary conditions associated with the beam #2. At $x_2 = L_{B2}$, $y_2(L_{B2}) = y_1(0)$ and the resulting deflection at the same point is given by:

$$\alpha_2(L_{B2}) = \alpha_1(0) + \phi \quad \phi = \frac{PL_{B2}}{k_T} \tag{22}$$

where ϕ is the deflection due to the torsional spring. Thus,

$$\begin{aligned} C_3 &= \frac{PL_{B2}}{k_T} - \frac{P}{EI}\left(\frac{L_{B2}^2}{2} + \frac{L_{B1}^2}{2} + L_{B1}L_{B2}\right) \\ C_4 &= \frac{P}{EI}\left(L_{B1}^2L_{B2} + \frac{L_{B1}^3}{3} + \frac{L_{B2}^3}{3} + L_{B1}L_{B2}^2\right) - \frac{PL_{B2}^2}{k_T} \end{aligned} \tag{23}$$

At $x_2 = 0$, $k_{B2} = P/y_2$. Consequently,

$$k_{B2} = \frac{1}{\frac{1}{EI}\left(L_{B1}^2L_{B2} + \frac{L_{B1}^3}{3} + \frac{L_{B2}^3}{3} + L_{B1}L_{B2}^2\right) - \frac{L_{B2}}{k_T}} \tag{24}$$

Substituting Eqs. (24), (20), and (13) into Eq. (15), the equivalent stiffness of the blade with crack is obtained.

3 Numerical Application

The goal of this work was to analyze the influence of a crack on the dynamic behavior of a rotor-blade system. Equation (11) was solved by considering two structural conditions, namely healthy blades (pristine condition) and a crack placed in the blade #1 distant $L_{B1} = 0.05\ L_1$ from its root (i.e., the point where the blade is attached to the rotor). Table 1 presents the parameters of the considered rotor-blade system.

Table 1. Parameters of the rotor-blade system.

Rotor			Blades (i = 1, 2, 3, 4)		
m_r	1.907	kg	θ_i	$(i-1)\pi/2$	rad
k_y	2.16×10^4	N/m	m_{pi}	0.1*	kg
r	0.04	m	k_i	1012	N/m
E	2×10^{11}	N/m^2	L_i	0.2	m
ε	1×10^{-5}	m	b_{ti}	0.006	m
Φ	0	rad	h	0.003	m
			L_{ti}	0.03	m
			r_{ti}	0.015	m
			I_{ti}	7.575×10^{-6}	kg m^2
			E	$2x10^{11}$	N/m^2
			I_i	1.35×10^{-11}	m^4

*Tip mass attached to the blade.

Figure 3 shows the vibration modes and corresponding natural frequencies of the healthy rotor-blade system. Note that the fourth and fifth modes are associated with the coupling between the rotor and the blades. The remaining vibration modes are associated with the blades motion.

Table 2 presents the parameters of the crack included in blade #1. This configuration was chosen aiming at emphasizing the effect of the crack brings on the dynamic behavior of the system. Figure 4 presents waterfall diagrams for which frequency responses functions were obtained in blade #1 according to the rotation speed of the rotor-blade system. Curves A and C represent the natural frequencies for the blade #1 with 25% and 50% crack depths, respectively. Curves B and D correspond to the same natural frequencies associated with the healthy system. As expected, the crack presence results in smaller natural frequencies as compared with the pristine condition. Additionally, the difference between the curves increases according to the crack depth. It is worth mentioning that the crack presence leads to a classic case of mistuning since the natural frequencies of the healthy and damaged blades become different [14]. Thus, unstable behavior may happen.

In this context, it is interesting to perform an instability analysis to evaluate the influence of the crack presence. The real parts of the system eigenvalues were analyzed [15], in which positive values indicate unstable condition. This study was performed by varying the rotation speed from 0 to 2500 RPM (in steps of 10 RPM) and the crack depth from 0 to 50% (in steps of 5%) of the blade height. In the present work, two different cases were analyzed. The first one is associated with the open crack (always-open crack during the simulation process - constant stiffness reduction of the blade #1). In the second case, the crack was able to open and close abruptly (breathing crack), according to the displacement of the blade #1 tip (see $z_1(t)$ in Fig. 1).

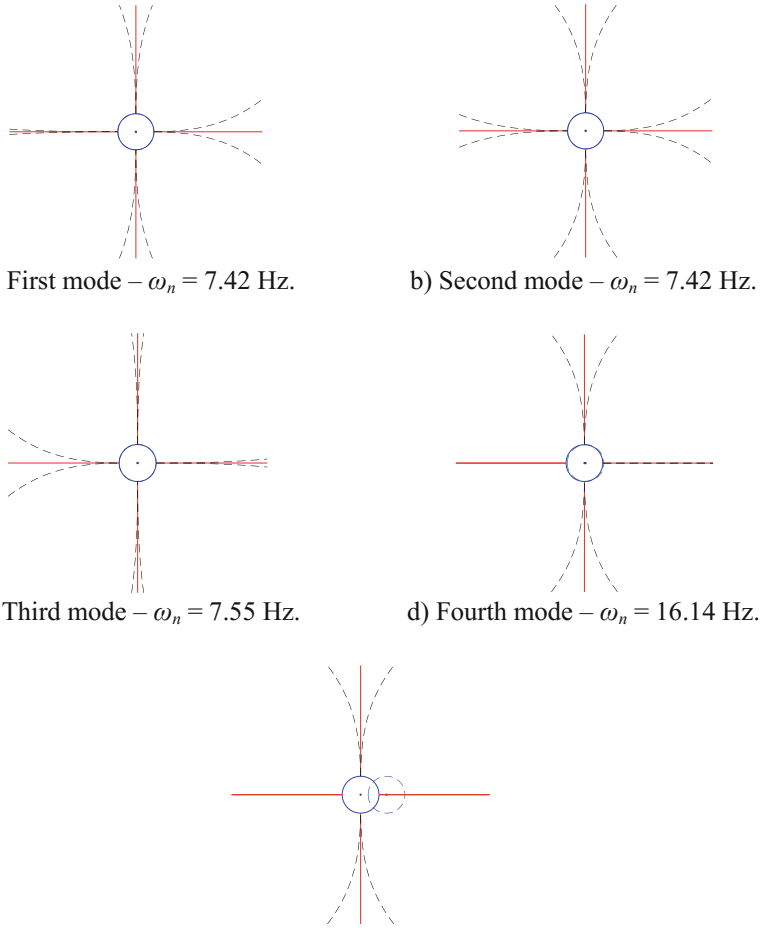

a) First mode – $\omega_n = 7.42$ Hz.

b) Second mode – $\omega_n = 7.42$ Hz.

c) Third mode – $\omega_n = 7.55$ Hz.

d) Fourth mode – $\omega_n = 16.14$ Hz.

e) Fifth mode – $\omega_n = 16.14$ Hz.

Fig. 3. Vibration modes and corresponding natural frequencies of the healthy sytem.

Table 2. Parameters of the crack model.

Pristine condition			25% crack depth			50% crack depth		
k_{eq}	1012	N/m	k_{eq}	650	N/m	k_{eq}	261	N/m
a/h	0		a/h	0.25		a/h	0.5	
L_{B1}	0.2	m	L_{B1}	0.01	m	L_{B1}	0.01	m
L_{B2}	0	m	L_{B2}	0.19	m	L_{B2}	0.19	m

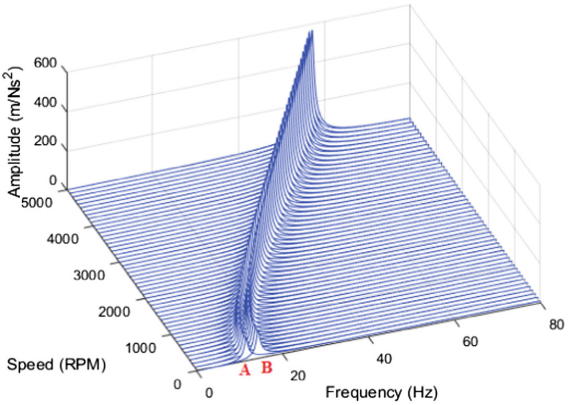

a) 25% crack depth.

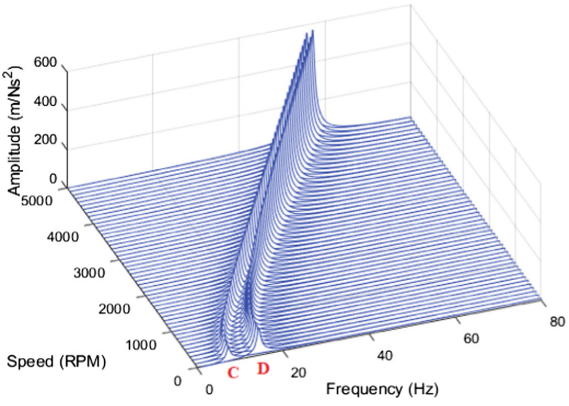

b) 50% crack depth.

Fig. 4. Waterfall diagrams for the blade #1 by considering two crack depths.

To introduce the breathing in the model was considered in Eq. (11), Positive displacements indicate a full closed crack (pristine condition) and negative values leads to a full open crack (stiffness reduction). Regarding the results for the instability regimes, for both cases (open crack and breathing crack) a new eigenvalue problem was solved for each time-step. Then, the real part of the eigenvalues where checked as a criterion for stability. For the breathing crack condition, the crack changes from closed (healthy blade) to open along the simulation. The unstable condition was observed only when the breathing crack is open. Thus, regarding the stability of the system, it is expected that the same result be obtained for both crack conditions, as can be seen in Fig. 5.

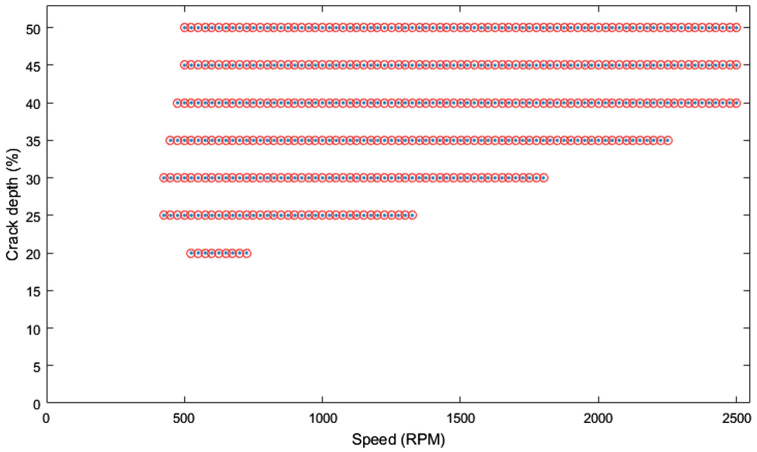

Fig. 5. Stability map of the rotor-blade system by considering the full open (•) and the breathing crack (o).

It is important to highlight that the unstable condition was associated only to the fourth and fifth vibration modes (see Fig. 3; positive real part obtained only in the eigenvalues of the fourth and fifth modes), and these conditions were obtained for crack depths above 20%.

Figures 6, 7 and 8 show the displacement of the blade #1 tip (see $z_1(t)$ in Fig. 1) with the system operating at 250 RPM, 970 RPM, and 2000 RPM, respectively, where 25% and 50% crack depths in blade #1 are considered, as well as its pristine condition. Stable and unstable conditions were achieved for these cases, as presented by Table 3 (see Fig. 5). The rotor-blade system was simulated for 20 s. Note that the vibration responses obtained by considering the full open and breathing cracks are different for 250 RPM and 970 RPM, mainly for the lower speeds for which a 50% breathing crack introduce a new peak in the response. However, similar results were obtained with the rotor-blade system operating at 2000 RPM, which agrees with the waterfall diagram,

Table 3. Stable and unstable conditions according to the rotation speed.

Crack depth	25%	50%
250 RPM	Stable	Stable
970 RPM	Unstable	Unstable
2000 RPM	Stable	Unstable

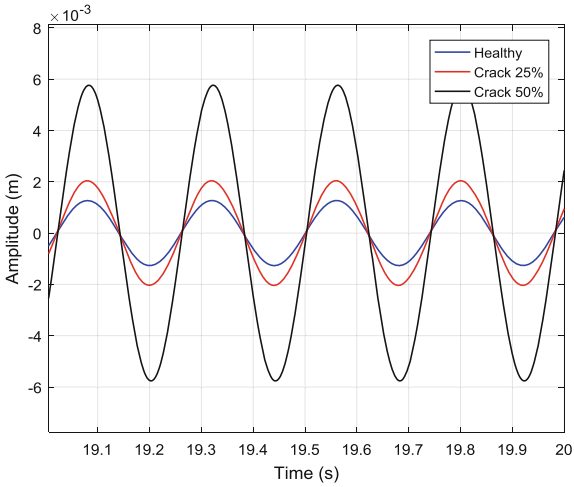

a) full open crack.

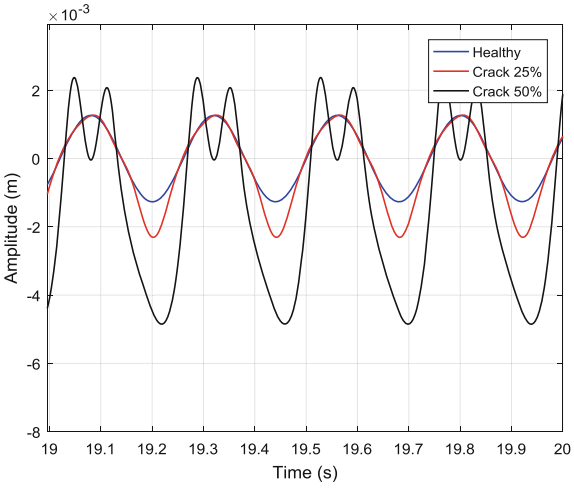

b) breathing crack.

Fig. 6. Vibration responses obtained with the system operating at 250 RPM.

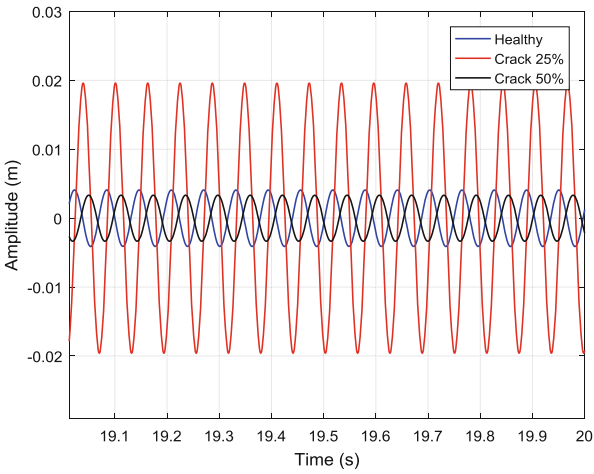

a) full open crack.

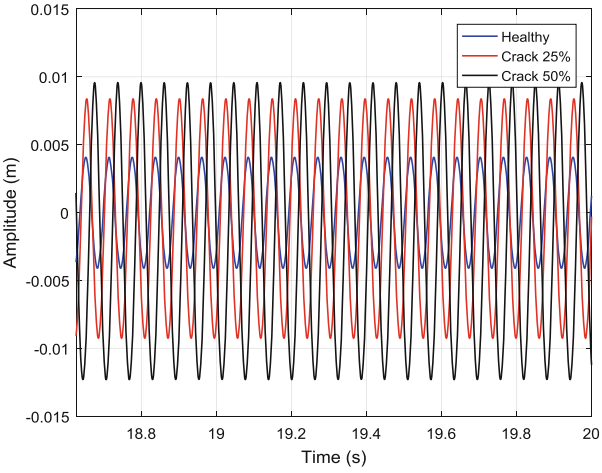

b) breathing crack.

Fig. 7. Vibration responses obtained with the system operating at 970 RPM.

since the two curves shown in Fig. 4 get closer due to the rotation increase. Additionally, it can be observed that the vibration amplitude does not increase necessarily with the crack depth (see Figs. 7a and 8a, b).

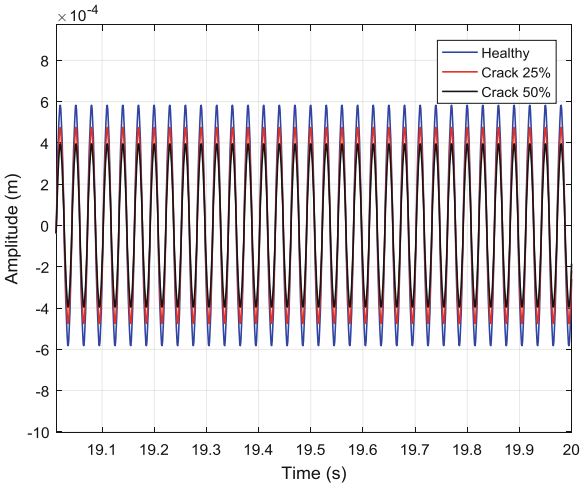

a) full open crack.

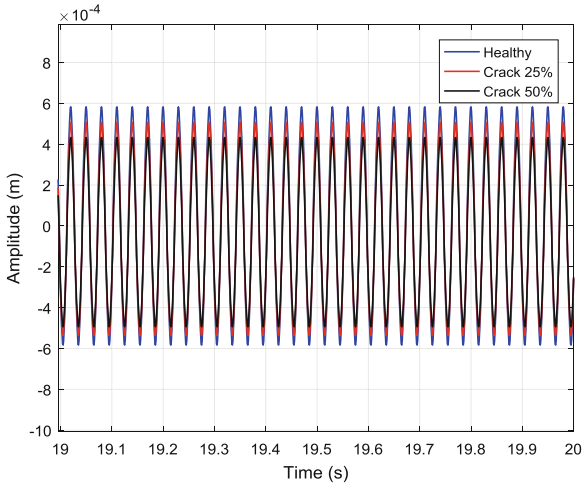

b) breathing crack.

Fig. 8. Vibration responses obtained with the system operating at 2000 RPM.

4 Conclusions

It is well known that rotating machines coupled with blades may operate under certain conditions that can lead to the growth of cracks. The presence of cracks is undesirable since it may lead to the failure of the system.

Thus, it is necessary to apply predictive maintenance techniques as based on vibration responses to ensure safety operating conditions of these machines. In this context, this contribution demonstrated the effects that a crack introduced in a blade presents on the dynamic behavior of a rotor-blade system. From the results, it was

observed that the crack introduced local flexibility in the blade, which makes the system unstable. Full open and breathing crack behaviors were analyzed. It was demonstrated that the resulting stability map is the same for both crack conditions. The time vibration responses of the system were also evaluated, revealing that the full open and breathing crack induce different dynamic behaviors on the system. Further research effort will be dedicated to the experimental verification of the presented results.

Acknowledgments. The authors are thankful to the Brazilian Research Agencies CAPES, CNPq (574001/2008-5/304546/2017-8) and FAPEMIG (TEC-APQ-022284-15/TEC-APQ-307609) for the financial support provided to this research effort. The authors are also thankful to the companies CERAN, BAESA, ENERCAN, and Foz do Chapecó for the financial support through the R&D project *Robust Modeling for the Diagnosis of Defects in Generating Units* (02476-3108/2016).

References

1. Xu, H., Chen, Z., Xiong, Y., Yang, Y., Tao, L.: Nonlinear dynamic behaviors of rotated blades with small breathing cracks based on vibration power flow analysis. J. Shock Vib. **2016** (2016)
2. Wu, M.C., Huang, S.C.: On the vibration of cracked rotating blade. J. Shock Vib. **5**, 317–323 (1998)
3. Saavedra, P.N., Cuitiño, L.A.: Crack detection and vibration behavior of cracked beams. J. Comput. Struct. **79**(2001), 1451–1459 (2001)
4. Legrand, M.: Modèles de prèdiction de l'interaction rotor/stator dans un moteur d'avion. Doctorat, thesis, L'École Centrale de Nantes et l'Université de Nantes, Nantes (2005)
5. Santos, I.F., Saracho, C.M., Smith, J.T., Eiland, J.: Contribution to experimental validation of linear and non-linear dynamics models for representing rotor-blade parametric coupled vibrations. J. Sound Vib. **271**, 883–904 (2004)
6. Saracho, C.M.: Numerical and experimental analysis of flexible blade dynamic behavior. Campinas State University. Thesis (Doctorate), Campinas (2002)
7. Dimarogonas, A.D.: Vibration Engineering. St. Paul, West Publishers (1976)
8. Chondros, T.G.: Dynamic response of a cracked beam. University of Patras, Greece. M.Sc. thesis (1977)
9. Dimarogonas, A.D., Rizos, P.F., Aspragathos, N.: Identification of crack location and magnitude in a cantilever beam from the vibration modes. J. Sound Vib. **138**, 331–338 (1990)
10. Dimarogonas, A.D., Paipetis, S.A.: Analytical Methods in Rotor Dynamics. Elsevier, London (1983)
11. Mayes, I.W., Davies, W.G.R.: Analysis of the response of a multi-rotor-bearing system containing a transversal crack in a rotor. J. Vib. Acoust. Stress Reliab. Des. **106**, 139–146 (1984)
12. Simo, J.C., Vu-Quoc, L.: On the dynamics of flexible beams under large overall motion—the plane case. Part I and II. ASME J. Appl. Mech. **53**, 849–863 (1986)
13. Kane, T.R., Ryan, R.R., Banerjee, A.K.: Dynamics of a cantilever beam attached to a moving base. J. Guid. Control Dyn. **10**(2), 139–151 (1987)
14. Choi, Y.S., Gottfried, D.A., Fleeter, S.: Analysis of structural mistuning effects on bladed disc vibrations including aerodynamic damping. In: International Compressor Engineering Conference. Paper 1627 (2004)
15. Ogata, K.: Modern Control Engineering, 4th edn. Prentice Hall, Upper Saddle River (2002)